Anomalous metallic lithium phases: Identification by ESR, ENDOR, and the bistable Overhauser effect

C. Vigreux, P. Loiseau, L. Binet, and D. Gourier*
Ecole Nationale Supérieure de Chimie de Paris (ENSCP), Laboratoire de Chimie Appliquée de l'Etat Solide, 11 rue Pierre et Marie Curie, 75231 Paris Cedex 05, France
(Received 14 May 1999)

Metallic lithium particles precipitated in lithium hydride by UV irradiation are investigated by electron spin resonance (ESR), electron-nuclear double resonance (ENDOR), and ESR at low temperatures under conditions of bistable Overhauser effect [Phys. Rev. B **47**, 15 023 (1993)]. Although the conventional ESR spectroscopy gives only a single structureless line for conduction electrons, ENDOR clearly shows the existence of two well-defined populations of lithium particles with different crystallographic structures. The presence of a quadrupole structure in the ENDOR spectrum indicates that one of the two populations belongs to the $9R$ close-packed phase of metallic lithium, normally stable below 80 K. The other population belongs to a cubic phase. At low temperatures the saturation of the ESR line produces a bistable Overhauser effect which gives a hysteresis of the ESR trace. This bistable conduction electron spin resonance clearly confirms the existence of two different populations of lithium particles. The presence of a broad hysteresis of the resonance at 4 K is the consequence of a very long T_2, which amounts to 5×10^{-6} s and 10^{-6} s in the cubic and the noncubic phases, respectively. These values are much larger than those deduced from the linewidth of the unsaturated ESR line. It is concluded that ENDOR combined with bistable ESR could provide very selective methods for the investigation of the lithium anode in lithium batteries.

I. INTRODUCTION

Lithium is the lightest metal element, with the dramatic consequence that the spin-orbit coupling is so weak that lithium is one of the few metals giving an electron spin resonance (ESR) signal.[1] The ESR line is often so narrow that minute amounts of lithium can be detected despite the weak Pauli paramagnetism inherent to metals. For these reasons a lot of work has been devoted to the electron magnetic resonance of lithium, since the early days of the ESR.[2]

Particular interest has been shown to irradiated lithium compounds, characterized by the precipitation of lithium particles of variable size and shape. The most investigated system was LiF irradiated by thermal neutrons, where Li particles have been detected by x-ray diffraction,[3] NMR,[4] ESR,[5,6] and thermal analysis.[7] The very pure Li metal thus produced is so well protected from oxidizing ambient atmosphere and stable in time that neutron-irradiated LiF (hereafter referred to as LiF:Li) is frequently used as ESR intensity marker.[8] These pioneering works were initially motivated by the lithium breeding properties of lithium nucleus. This field of research is still active, with several recent works focused on Li_2O, considered as a potential first-wall cladding material for fusion reactors.[9] Careful observations by electronic and optical microscopies, ESR, and microwave conductivity measurements have recently been conducted on electron-irradiated Li_2O (hereafter referred to as Li_2O:Li) by Beuneu and co-workers.[10–13] ESR was essential in all these works, because the ESR line shape of metals depends mainly on the particle size a. For a larger than the skin depth δ of the metal at the microwave frequency ν (δ is of the order of a micrometer for lithium at room temperature and at X band), the ESR line shape exhibits the so-called Dysonian distorsion.[1] The line shape is Lorentzian for $a<\delta$. These two types of particles were clearly evidenced in Li_2O:Li single crystals by their very different linewidths and saturation behaviors.[11,12] The paramagnetism is of the Pauli type in both regimes. When metallic particles are so small that the difference between the adjacent electron energy levels at the Fermi level becomes much larger than kT, the paramagnetism exhibits a T^{-1} behavior and g distribution. This situation is referred to as quantum size effect (QSE) regime.[14] It occurs for a very small particle size, typically $a\leqslant5$ nm,[15] and has been clearly identified in LiF:Li.[16]

However, standard ESR spectroscopy suffers from shortcomings for complex systems containing associations of lithium precipitates with various shapes and sizes, impurity contents, or crystallographic structures. The difficulty is particularly evident when the precipitates exhibit a more or less Lorentzian resonance line at $g\approx2.0022$ with similar linewidths, the resultant line always appearing as nearly symmetrical and structureless. This clearly complicates the interpretation, the decomposition of the line into individual components being generally impossible despite some successful attempts. For example, a small deviation from the Lorentzian shape in the wings of the ESR line in LiF:Li at low temperatures was interpreted as the indication of a martensitic phase transition.[8] This lack of resolution and selectivity of lithium metal ESR hampers the use of this technique for the investigation of more complex systems such as lithium batteries, where lithium metal at the anode exhibits a complex behavior with dendritic growth upon charge-discharge cycles during the cell operation.[17]

Standard ESR spectroscopy can be implemented by using more selective electron magnetic resonance techniques based on the phenomenon of dynamic nuclear polarization (DNP) by the Overhauser effect.[18] A partial saturation of the ESR line of conduction electrons polarizes the nuclear spins, giv-

ing a nonzero nuclear field B_n which adds to the external field B_0, so that the resonance condition becomes

$$h\nu = g\beta(B_0 + B_n), \tag{1}$$

instead of $h\nu = g\beta B_0$ for an unsaturated ESR line. The well-known effect of DNP is a shift (Overhauser shift) of the ESR line. The Overhauser shift has been observed in metallic lithium at low temperatures in the early ESR studies on LiF:Li and in neutron-irradiated LiH (hereafter referred to as LiH:Li).[6,19] The nuclear field can be partially quenched by depolarizing the nuclei with a saturating radiofrequency field tuned to the appropriate nuclear frequency. This nuclear depolarization shifts back the ESR line to its unsaturated position, and thus modifies the ESR intensity at the value of the external magnetic field B_0. The ESR intensity change is an electron-nuclear double resonance (ENDOR) response. The first observation by ENDOR of this line shift mechanism has been made by Feher in the LiF:Li system.[20] This technique has been recently refined by Denninger and applied to a variety of conducting materials.[21,22] Owing to the high resolution (similar to NMR), the high sensitivity (similar to ESR) and the high selectivity of ENDOR, contributions of different phases of lithium indistinguishable in the ESR spectrum can be separated by this technique.

For strong DNP, i.e., for a large value of B_n in Eq. (1), the ESR line is also strongly distorted and deviates considerably from the Lorentzian shape.[23] An interesting situation arises when the electron spin-spin relaxation time T_2 and the nuclear field are sufficiently large to satisfy the following inequality:[24]

$$\gamma T_2 \Delta B_{ov}^{max} > 4, \tag{2}$$

where ΔB_{ov}^{max} is the highest nuclear field that can be achieved for given conditions of magnetic field and temperature. In this case the line shape depends on the sweep direction of the external field B_0, resulting in a hysteresis of the ESR line.[23,24] The line shapes of the increasing and decreasing sweep lines are very sensitive to electron relaxation times T_1 and T_2, to nuclear relaxation times T_{ln}, and to the hyperfine interaction between electron and nuclear spins.[23–25] Since hysteresis is the consequence of bistability, this situation will be hereafter referred to as bistable conduction electron-spin resonance (BCESR). It gives much more selective spectra than standard (unsaturated) ESR since lithium aggregates presenting different magnetic parameters give BCESR lines with different line shapes and positions. A characteristic BCESR spectrum has recently been reported for metallic Li particles in Li_2O:Li.[26]

We present in this paper a combined ESR-ENDOR-BCESR investigation of a lithium metal system for which the contributions of different types of lithium precipitates do not appear on the unsaturated ESR spectrum. We have chosen the LiH:Li system where Li precipitates are created by UV irradiation. In one of the early ESR works, Doyle, Ingram, and Smith showed that Li metal in this case is characterized by a strong symmetrical and narrow structureless ESR line, indicating the presence of submicronic Li particles.[27] In the present work the correlation between ENDOR, BCESR, and unsaturated ESR spectra clearly showed that this single, apparently simple system is actually formed of two very different populations of lithium particles characterized by well-defined magnetic parameters, revealing the coexistence of two crystallographically distinct phases of Li metal.

II. EXPERIMENTAL PART

The samples studied in this work were nominally pure 97% LiH powder purchased from Fluka. Owing to the high reactivity of LiH with water, all manipulations were made under argon in a glovebox. The average grain size of the powder was about 10 μm. Preliminary ESR characterization of the unirradiated samples always showed a Dysonian signal typical of metallic lithium. In order to eliminate this residual lithium, all the samples were treated under argon/hydrogen (90/10) flux in a SiO_2 crucible. The temperature was increased at a rate of 300 °C/h up to 600 °C kept at this value during 1 h, and then lowered at a rate of 300 °C/h. The powder being slightly sintered by this treatment, the samples were always ground before irradiation. We often observed the growth of LiH single crystals during the annealing treatment. The samples were irradiated at room temperature with a mercury lamp delivering a maximum power of 640 W, and equipped with a water filter and a condenser. They were placed at about 2 cm from the lamp, and the homogeneity of the irradiation was ensured by rotating the sample tube during irradiation.

ESR spectra were recorded with a Bruker ESP 300 spectrometer operating at X band with a standard TE_{102} cavity. The microwave frequency was measured with a precision of 10^{-5} GHz, which corresponds to an uncertainty of about 3.5×10^{-4} mT on the ESR line position. The spectra were recorded from 4 to 100 K with an Oxford Instruments helium flow cryostat, and with a standard nitrogen flow system for higher temperatures. The incident microwave power P at the sample is related to the microwave field B_1 at the sample by $P = KB_1^2$, where the cavity constant K is equal to 4.0×10^4 mW mT^{-2} and 5.2×10^4 mW mT^{-2} when the cavity is equipped with the helium and nitrogen inserts, respectively. ENDOR spectra were recorded at room temperature with the Bruker cavity working in the TM_{110} mode. No ENDOR response could be obtained with frequency modulation of the radiofrequency (rf) carrier, as is generally the case for ENDOR of molecular radicals and defects in solids. However, high ENDOR enhancement was obtained with a 12.5-kHz modulation of the applied magnetic field.

III. ESR RESULTS

We describe in this part the results of standard ESR spectroscopy, characterized by low incident microwave power which precludes any DNP by the Overhauser effect. For metallic lithium at room temperature this situation is achieved at microwave power of the order of 0.1 mW or less. Figure 1(a) shows an example of an ESR spectrum recorded at room temperature for a LiH powder sample irradiated during 3 h at room temperature. The very narrow and almost symmetrical line (sample dependent linewidth $\Delta B = 8-15\ \mu$T) is similar to that observed by Doyle, Ingram, and Smith.[27] The linewidth is slightly dependent on the irradiation time as it decreases from $\approx 20\ \mu$T to $\approx 8\ \mu$T when the irradiation time varies from $\leqslant 0.25$ to 6 h. It is now largely proved that such

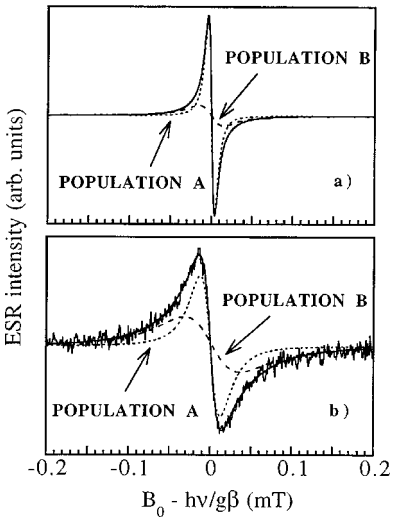

FIG. 1. Example of experimental and simulated ESR spectrum at room temperature for a LiH powder sample irradiated during 3 h. Microwave power $P=5\ \mu$W, (a) just after irradiation: the dotted and discontinuous lines represent population A ($\Delta B=8.4\ \mu$T, 40%) and population B ($\Delta B=31\ \mu$T, 60%), respectively; (b) after annealing at 180 °C during 500 min: the dotted and discontinuous lines represent population A ($\Delta B=25.3\ \mu$T, 26%) and population B (($\Delta B=68.8\ \mu$T, 74%), respectively. The resulting simulations are indistinguishable from the experimental spectra.

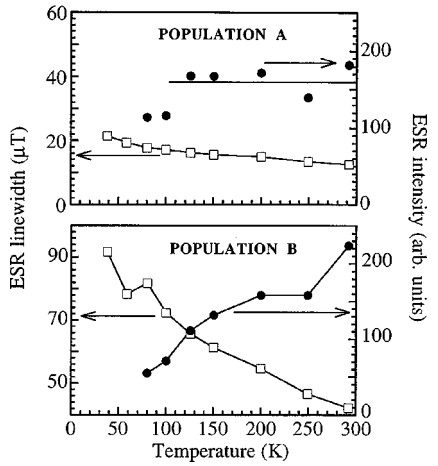

FIG. 2. Temperature dependence of the ESR linewidth (empty squares) and intensity (full circles) for populations A and B in a LiH powder sample irradiated during 3 h.

narrow lines are due to metallic lithium particles of size a (diameter for a sphere, thickness for a platelet) smaller than the skin depth δ of the metal at X band. The ESR linewidths measured in the present work are very similar to those found in Li_2O:Li ($\Delta B\approx 13\ \mu$T),[10,11] but smaller than the values generally measured for LiF:Li ($\Delta B\approx 56-65\ \mu$T).[8] The ESR lines in LiH:Li are however broader than those observed with very pure lithium films precipitated from liquid-ammonia solutions, characterized by $\Delta B\approx 2\ \mu$T.[28]

Despite its apparently structureless and symmetrical shape, the ESR line in Fig. 1(a) could not be simulated with a simple Lorentzian shape function as expected for a single population of lithium particles.[1] A much better agreement was obtained by fitting the ESR line to the sum of a narrow ($\Delta B\approx 8.4\ \mu$T) and a broad ($\Delta B\approx 31\ \mu$T) Lorentzian lines centered at $g=2.0022$, corresponding to two sets of lithium particles, hereafter referred to as populations A and B. Exactly the same situation was encountered with LiH single crystals, with a two-component ESR line invariant upon rotation of the magnetic field. This indicates that lithium particles are located in the bulk of the crystallites. Careful examination of the spectra shows that the narrow line (population A) is Lorentzian while the broad line (population B) is often slightly distorted with a small amount of Dysonian character, indicating that the particle size might be larger in population B than in population A. The linewidths and the relative intensities of ESR components A and B are slightly dependent on the irradiation time. Population B always dominates with a ratio B(%)/A(%) varying from 90/10 to 60/40 for irradiation times increasing from $\leqslant$0.25 to 6 h. Correlatively the linewidths of populations B and A decrease from 60 to 30 μT and from 20 to 8 μT, respectively. It is important to note that ESR alone cannot demonstrate the existence of two distinct populations of lithium particles, as the spectrum of Fig. 1(a) may well be simulated also by a sum of more than two lines. The presence of two well-defined populations could only be proved by the effect of DNP at room and low temperatures, responsible of the ENDOR and the BCESR spectra described in the following sections. For the moment we only postulate the existence of these two sets of particles.

Figure 2 shows the temperature dependence of the peak-to-peak linewidth ΔB and the ESR intensity for populations A and B, as deduced from the two-component simulation. The intensities were measured by double integration of the simulated components of the ESR line. The linewidth for population A weakly depends on temperature as ΔB increases from $\approx$10 to $\approx$20 μT when T decreases from room temperature to 40 K. This small broadening is partly due to the onset of DNP at low temperature, which distorts and broadens the ESR lines.[23] In the same temperature range, the linewidth of population B increases from $\approx$40 to $\approx$90 μT. The ESR intensity of population A does not depend on temperature between room temperature and 100 K, and appears to decrease slightly below this temperature (Fig. 2). This behavior is consistent with the Pauli paramagnetism of metallic lithium, and the small decrease below 100 K is due to the effect of DNP.[23] Alternatively the ESR intensity for population B decreases by a factor 4 between room temperature and 70 K (Fig. 2). It is interesting to note that the temperature dependence of both ESR intensity and linewidth for populations A and B are similar to those found by Beuneu and Vajda for small and large lithium particles in Li_2O:Li single crystals.[11]

The ESR line shape also depends on the annealing effect on the irradiated samples. Figure 1(b) shows the effect of a 500-min annealing treatment at 180 °C of the sample of Fig. 1(a). The variation of ΔB and of the intensities versus the annealing time are plotted in Fig. 3. The following evolution is observed: (i) The linewidth increases from 10 to about 25 μT for population A and from 30 to 70 μT for population B, the same effect being observed for a treatment at a lower temperature (120 °C); (ii) The ESR intensity of the two populations decreases during the first 100 min of treatment and then stabilizes; (iii) the relative weight of population B

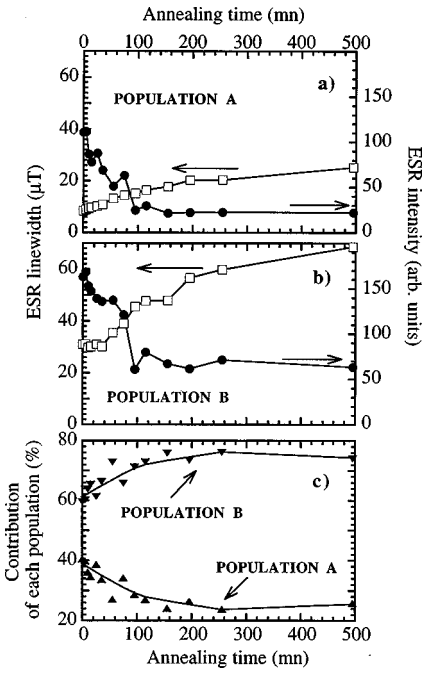

FIG. 3. Isothermal annealing behavior at $T=180\,^{\circ}\mathrm{C}$ of the ESR parameters of metallic Li in a LiH powder sample irradiated during 3 h; (a) and (b) ESR linewidths (open squares) and absolute intensities (full circles) for populations A and B; (c) contributions of each population to the total intensity.

increases by annealing; (iv) the line shape remains Lorentzian for population A while the weakly dysonian line shape of population B remains unchanged, with an asymmetry parameter[1] equal to about 1.2.

All these observations show that population B always dominates over population A, especially at low irradiation and long annealing times. The line broadening produced upon increasing the annealing treatment can be correlated to the line narrowing observed upon increasing the irradiation time, assuming that the linewidth is dominated by relaxation at the particle surface,[2] with particle size increasing during irradiation and decreasing during annealing treatment. It thus appears that population B is more favorable kinetically and more stable thermodynamically. The fact that the ESR line A is always Lorentzian whatever the irradiation time or the annealing time indicates that these particles are always much smaller than the skin depth of lithium at 4 K, i.e., $a \ll 0.12\,\mu\mathrm{m}$. Alternatively the ESR line B is always slightly Dysonian, indicating that lithium particles are larger in population B than in population A.

The particle size for population B can be estimated by line-shape analysis. Webb extended the Dyson theory to particles with ratios a/δ between 0.1 and 10.[29] The rather complicated expressions derived by this author were simplified by Berim *et al.* when the conditions $(DT_2)^{1/2} \gg \delta$ and $a \ll 20\delta$ are fulfilled, D and T_2 being the electron diffusion coefficient and the spin-spin relaxation time, respectively.[30] The first condition always holds for lithium while the second applies for particles of populations A and B. Under these conditions, the ESR line for the two populations is simply the sum of Lorentzian shaped absorption χ'' and dispersion χ' contributions. The following expression was obtained for a first derivative ESR line:[30]

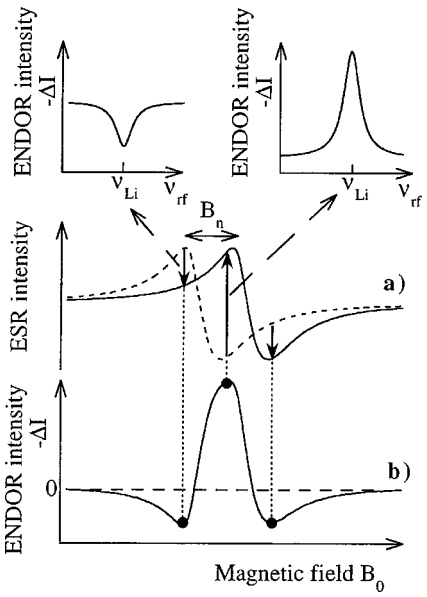

FIG. 4. Schematic representation of the ENDOR mechanism for metallic lithium particles. (a) unsaturated (full line) and saturated (discontinuous line) ESR transitions. The arrows represent the variations of the ESR intensity at three selected magnetic-field values B_0, induced by a saturating radiofrequency (ν_{rf}) field tuned to the nuclear frequency ν_{Li}^0 of ^{7}Li nucleus. The ENDOR intensities are proportional to the lengths of the arrows. Two ENDOR responses are also shown in the top of the figure. (b) Magnetic field dependence of the ENDOR intensity.

$$\frac{dP}{dB_0} = \alpha \frac{1-x^2}{(1+x^2)^2} - \beta \frac{2x}{(1+x^2)^2}, \tag{3}$$

with $x=\gamma(B-B_0)T_2$, and γ is the electron gyromagnetic ratio. By using Eq. (3) for population B and a purely Lorentzian shape for population A [Eq. (3) with $\alpha=0$ and $\beta=1$], a simulation of excellent quality of the experimental spectra was always obtained. Parameters α and β determine the asymmetry of the ESR line, and are directly related to the ratio a/δ.[30] Simulation of the ESR line B with Eq. (3) and expressions given by Berim *et al.* show that the particle size for population B is of the order of 0.6 μm. The decrease of the ESR intensity with temperature [Fig. 2(b)] is also consistent with the Dysonian character of the ESR line of population B, as a thinner part of the particles is observed when δ decreases with T, following the $\sigma^{-1/2}$ dependence of δ.[11]

IV. ENDOR RESULTS

A. Background

In this part we describe with some details the ENDOR results, as this technique gave the unequivocal proof of the existence of two distinct populations of lithium particles, and provided informations on their crystallographic structures. In order to clarify the rather complex ENDOR behavior of LiH:Li shown in Sec. IV B, let us first consider the theoretical ENDOR response of a homogeneous population of lithium particles of size $a<\delta$, characterized at room temperature by a Lorentzian ESR line. At very low microwave power ($P<0.1\,\mathrm{mW}$), this line is centered at the resonance field $h\nu/g\beta$ [Fig. 4(a), full line]. At higher microwave

power, the ESR line is partially saturated and shifts to low field with respect to the unsaturated one by the nuclear field B_n induced by the DNP [Fig. 4(a), discontinuous line; see also Eq. (1)].[18] Assuming that the DNP does not affect significantly the line shape, which is the case at room temperature with LiH:Li, the unsaturated ESR intensity $I(B_0)$ at a given value B_0 of the external magnetic field is thus modified by the DNP by the quantity $\Delta I(B_0)=I(B_0)-I(B_0+B_n)$, which can be either positive or negative depending on the value of B_0 [see Fig. 4(a)]. The nuclear field responsible for this shift can be quenched by applying a saturating radiofrequency (rf) radiation $\nu_{\rm rf}$ tuned to the nuclear frequency $\nu^0_{\rm Li}=g_n\beta_n B_0/h$ of ^{7}Li nuclei (92.5% natural abundance, $I=\frac{3}{2}$, $g_n=2.170\,961$). Thus if the external magnetic field is set at a value B_0 while saturating the ESR line and scanning $\nu_{\rm rf}$, the ESR intensity will make a jump equal to $-\Delta I(B_0)$ for $\nu_{\rm rf}=\nu^0_{\rm Li}$. This ENDOR response may be positive or negative depending on the field setting B_0. The arrows in Fig. 4(a) represent the magnitude and the sign of the ENDOR signal $-\Delta I(B_0)$ for three examples of field setting values. If the nuclear spin lattice relaxation time T_{1n} responsible for the DNP is larger than the spin-spin relaxation time T_{2n}, which is the case with metallic Li at room temperature,[31] the theoretical ENDOR response $-\Delta I(B_0)$ has the form of a positive or negative symmetrical line. Two examples are shown on top of Fig. 4(a). Thus the amplitude and the sign of the ENDOR response strongly depend on B_0, as shown in Fig. 4(b) representing the variation of the ENDOR intensity $-\Delta I(B_0)$ as a function of the field B_0. The base line (discontinuous line) corresponds to the polarized ESR intensity $I(B_0+B_n)$. This curve has roughly the shape of a second derivative of the ESR absorption. We will use in the next part the simple situation described in Fig. 4 to interpret the more complex ENDOR response of LiH:Li.

B. ENDOR of LiH:Li

Figure 5 shows an ESR spectrum and some representative ENDOR spectra at room temperature for a powder LiH:Li sample irradiated during 3 h. Each ENDOR trace corresponds to a particular field setting B_0, indicated by open circles on the ESR spectrum of Fig. 5. The striking feature of the ENDOR response of Li metal is that its shape exhibits a considerable field setting dependence. When the field B_0 is set in the left side of the ESR spectrum [field setting a, Fig. 5(a)], the ENDOR response is a narrow negative line at the nuclear frequency of Li ($\nu^0_{\rm Li}\approx 5.66$ MHz). When B_0 is shifted to a value close to the maximum of the ESR line [field settings b and c, Figs. 5(b) and 5(c)], a broad positive line is superimposed on the narrow negative line [Fig. 5(b)]. A very small increase of the field setting results in a strong decrease of the narrow line [Fig. 5(c)] which then becomes positive and largely dominates the broad line [Figs. 5(d) and 5(e)] when the field is set in the central part of the ESR line. A further increase of the field setting gives the same ENDOR features as for the low field setting case. First, the narrow positive line decreases more rapidly than the broad line and becomes negative, while the broad line remains positive [Fig. 5(f)]. Increasing B_0 again results in the increase of the negative line while the broad line decreases and becomes negative [Fig. 5(g)].

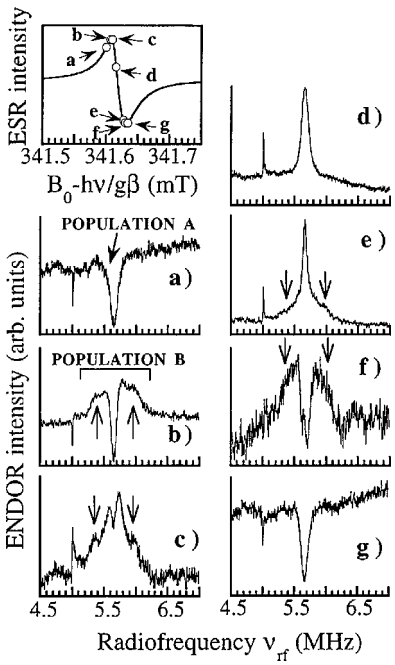

FIG. 5. Selected ENDOR spectra recorded at room temperature and at different values of the magnetic field [(a)–(g)]. Each field setting is marked by an empty circle on the partially saturated ESR spectrum shown in the top of the figure. The narrow and broad ENDOR lines represent the responses of populations A and B, respectively. The features indicated by arrows show the apparent quadrupolar structure of the ENDOR trace of population B. Microwave power $P=40$ mW; radiofrequency power 100 W, modulation frequency: 12.5 kHz; modulation depth 5 μT.

All these features can be explained only if we assume that the ESR line is actually the overlap of a narrow and a broader line representing two separate populations of lithium particles, as postulated in Sec. III. Each ESR line gives an independent ENDOR response which can be either positive or negative, depending on the field setting as previously shown in Fig. 4. The theoretical variation of the ENDOR intensity $-\Delta I(B_0)$ versus B_0 is shown in Fig. 6 in the case of two overlapping ESR lines corresponding to populations A and B. The different field setting values B_0 corresponding

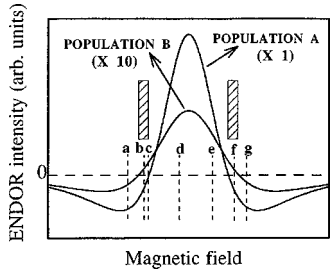

FIG. 6. Schematic representation of the theoretical magnetic-field dependence of the ENDOR intensity of populations A and B. The curve for population B is amplified with respect to that of population A. The base line (discontinuous line) is the zero ENDOR intensity. The ENDOR responses of populations A and B are negative and positive, respectively, in the two narrow magnetic-field ranges represented by dashed areas. The ENDOR intensities of the two populations are either positive or negative outside these domains.

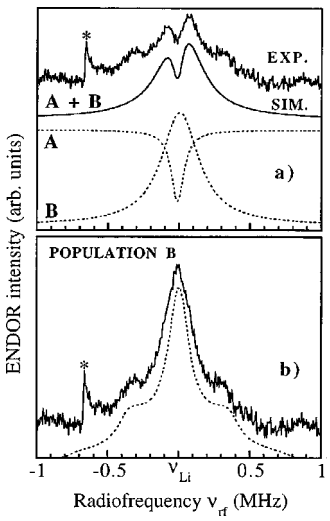

FIG. 7. (a) Experimental ENDOR spectrum recorded with the field setting c of Fig. 5. The full line represents a simulation of the middle part of the spectrum by the sum of a negative line for population A and a broader positive line for population B. The two individual components (dotted lines) are Lorentzian. (b) Spectrum of population B obtained by subtracting the negative line of population A from the experimental spectrum. The dotted line represents the simulation of the spectrum of population B by taking into account a quadrupole structure. The spurious feature indicated by a star is due to instrumental effect.

to the spectra of Figs. 5(a)–5(g) are also shown in Fig. 6. Since the base line (discontinuous line) represents a zero ENDOR intensity, it can be seen that the ENDOR responses are positive for population B and negative for population A in very narrow magnetic field ranges within the limits of the dashed areas in Fig. 6. Outside these peculiar field ranges, ENDOR lines are either positive or negative for the two populations.

The fact that the two overlapping ESR lines give distinct ENDOR responses shows that they belong to two separate electron-nuclear spin systems which are not connected by spin-relaxation mechanisms. In other words, the narrow and broad ESR/ENDOR line systems correspond to populations A and B, respectively.

C. ENDOR of population B

Let us now address the structural characterization of the two populations. For the moment we assume only that the particles are of submicron size in the two populations, and that the particles are slightly larger in population B than in population A. However, a difference in size cannot explain the behaviors of their ENDOR responses. A careful examination of all the ENDOR spectra shows that the narrow line of population A is structureless while the broad line of population B exhibits an apparent satellite structure indicated by arrows in Fig. 5. These satellites are more evident when the field setting is selected so that the narrow ENDOR line of population A almost vanishes. This is the case of Fig. 5(c). This particular field setting has been chosen for a more detailed analysis of the ENDOR line of population B, which can be simulated after subtraction of the residual contribution of population A. Figure 7(a) shows an expanded view of the ENDOR spectrum recorded with the field setting c. The spurious feature at 5 MHz is due to an instrumental effect. The residual contribution of population A was eliminated by simulating the experimental spectrum as the sum of a broad positive line representing population B and a narrow line for population A, both being Lorentzian shaped. The relative weight of these two lines was chosen to give an accurate reproduction of the middle part of the experimental spectrum [Fig. 7(a)]. The spectrum of population B was next reconstructed by subtracting the ENDOR line A from the experimental spectrum, which gave the spectrum of population B shown in Fig. 7(b).

The simulation of this spectrum used the general nuclear-spin Hamiltonian of ^{7}Li nuclei in a lithium particle:[31]

$$\mathcal{H}=-g_n\beta_n\mathbf{I}\cdot\mathbf{B}_0+\frac{e^2qQ}{4I(2I-1)}\times\left\{3I_Z^2-I(I+1)+\frac{1}{2}\eta(I_+^2+I_-^2)\right\}, \tag{4}$$

where the two terms represent the nuclear Zeeman interaction and the quadrupole interaction, respectively. We have neglected the hyperfine interaction between the conduction electron spin S and the nuclear spin I of the particle because this interaction is only responsible for a Knight shift of the ENDOR line which is much smaller than the ENDOR linewidth.[32] The quadrupole interaction appears for nuclei with spin $I>\frac{1}{2}$, (which possess an electric quadrupole moment eQ) experiencing an electric-field gradient of components V_{jj} characterized by $\Sigma_j V_{jj}=0$, with $j=X$, Y, and Z being the principal axes of the electric-field gradient tensor. The Z component of the electric-field gradient is $eq=V_{ZZ}$. For a quadrupole interaction smaller than the nuclear Zeeman interaction, which is the case with lithium particles, the nuclear-spin energy levels E_{m_I} of each spin state m_I can be obtained by a first-order perturbation treatment of Eq. (4):[33]

$$E_{m_I}=-g_n\beta_nB_0m_I+\frac{1}{4}h\nu_Q[3\cos^2\theta-1+\eta\sin^2\theta\cos 2\varphi]\times[m_I^2-I(I+1)/3], \tag{5}$$

where $\nu_Q=3eQV_{ZZ}/h2I(2I-1)$ is the quadrupole frequency and $\eta=(V_{XX}-V_{YY})/V_{ZZ}$ is the asymmetry parameter of the electric-field gradient. θ and φ are the polar angles of the field B_0. The three allowed NMR transitions $m_I-1\leftrightarrow m_I$ occur at frequencies $\nu_{m_I}=(E_{m_I-1}-E_{m_I})/h$. Without quadrupole interaction ($V_{XX}=V_{YY}=V_{ZZ}=0$), there is only one ENDOR frequency $\nu_{\mathrm{Li}}^0=g_n\beta_nB_0/h$. This situation corresponds to population A, which gives only a structureless ENDOR line and thus exhibits a cubic crystallographic structure. For a nonvanishing electric-field gradient, which is the case with population B, we expect three ENDOR lines at frequencies ν_1 ($\frac{3}{2}\leftrightarrow\frac{1}{2}$ transition), ν_2 ($\frac{1}{2}\leftrightarrow-\frac{1}{2}$ transition), and ν_3 ($-\frac{3}{2}\leftrightarrow-\frac{1}{2}$ transition) given by

$$\nu_1(\theta,\varphi)=\nu_{\mathrm{Li}}-\frac{\nu_Q}{2}(3\cos^2\theta-1+\eta\sin^2\theta\cos 2\varphi),$$
$$\nu_2(\theta,\varphi)=\nu_{\mathrm{Li}}, \tag{6}$$
$$\nu_3(\theta,\varphi)=\nu_{\mathrm{Li}}+\frac{\nu_Q}{2}(3\cos^2\theta-1+\eta\sin^2\theta\cos 2\varphi).$$

The ENDOR intensities, proportional to $|\langle m_I-1|I^+ + I^-|m_I\rangle|^2$, are in the ratio 3:4:3 for ν_1, ν_2, and ν_3, respectively. The resulting ENDOR spectrum is calculated by integrating over the polar angles θ and φ the sum of the three ENDOR lines:

$$I(\nu)=\int_{\theta=0}^{\pi} d\cos\theta\int_{\varphi=0}^{2\pi} d\varphi\sum_{i=1}^{3} p_i f(\nu-\nu_i(\theta,\varphi)). \tag{7}$$

The coefficients $p_i (i=1,2,3)$ are proportional to the transition probabilities, with $p_1=p_3=3$ and $p_2=4$. Each ENDOR transition has a Lorentzian shape $f(\nu-\nu_i(\theta,\varphi))=\{1+4[\nu-\nu_i(\theta,\varphi)]^2/(\Delta\nu)^2\}^{-1}$ where $\Delta\nu$ is the width at half height of the transition.

The ENDOR spectrum of population B shown in Fig. 7(b) was simulated with three adjustable parameters $\Delta\nu$, ν_Q, and η. The best fit was achieved with $\nu_Q=0.75$ MHz, $\Delta\nu=0.170$ MHz, and $\eta=0$, which indicates that the electric-field gradient at ^{7}Li site has an axial symmetry. The corresponding ENDOR parameters for population A are $\nu_Q=0$, $\Delta\nu=0.108$ MHz, and $\eta=0$. Thus the two populations have nearly the same ENDOR linewidths and differ only by the symmetry of the Li sites, which is cubic for population A and axial for population B. The consequences of these features are discussed in Sec. VI.

It is noteworthy that the ENDOR spectra of populations A and B are not centered at the same rf value, which results in a visible dissymmetry of the spectrum. This is particularly evident for spectra with two components of comparable intensities for each population [Figs. 5(b), 5(c), and 5(e)]. For example, the spectrum shown in Fig. 7 has been recorded at the field setting $B_0=341.88$ mT, corresponding to the nuclear Zeeman frequency $\nu^0_{\mathrm{Li}}=5.658$ MHz. The ENDOR spectra deduced from simulations [Fig. 7(a)] are centered at frequencies $\nu^{\mathrm{A}}_{\mathrm{Li}}\approx 5.659$ MHz and $\nu^{\mathrm{B}}_{\mathrm{Li}}\approx 5.675$ MHz for populations A and B, respectively. It thus appears that the central frequency of the ENDOR spectrum B is shifted by $+17$ kHz with respect to ν^0_{Li}. This shift is not due to a second-order effect of the quadrupole interaction because the latter is estimated to be -10 kHz, thus with the wrong sign. Also this shift is not due to a Knight shift of the nuclear resonance of population B, given by the following expression:[34]

$$K=\frac{\nu_{\mathrm{Li}}-\nu^0_{\mathrm{Li}}}{\nu^0_{\mathrm{Li}}}=\frac{8\pi}{3}\langle|\Psi_{\mathbf{k}}(0)|^2\rangle_F\chi_p M, \tag{8}$$

where $\langle|\Psi_{\mathbf{k}}(0)|^2\rangle_F$ is the average of $|\Psi_{\mathbf{k}}(0)|^2$ over the Fermi surface, M is the atomic mass, and χ_p is the magnetic susceptibility per mass unit. The Knight shift of metallic ^{7}Li amounts to $K=2.5\times10^{-4}$, thus the shift $\nu_{\mathrm{Li}}-\nu^0_{\mathrm{Li}}$ of the ENDOR frequency should be equal to $K\nu^0_{\mathrm{Li}}\approx 1$ kHz. This is an upper limit corresponding to electron spins at thermal equilibrium, and a partially saturated ESR transition should give an ENDOR shift $\nu_{\mathrm{Li}}-\nu^0_{\mathrm{Li}}<1$ kHz. Thus more experiments are needed to explain the ENDOR shift observed for population B.

V. BISTABLE CONDUCTION ELECTRON SPIN RESONANCE

A. Background

The nuclear field B_n due to the hyperfine interaction A of an electron spin with N nuclear spins in Eq. (1) is related to the nuclear polarization $\langle I_z\rangle$ by[6,18]

$$B_n=\frac{NA}{g\beta}\langle I_z\rangle. \tag{9}$$

At very low incident microwave power, the only source of nuclear polarization is the thermal equilibrium between the nuclear-spin states $\langle I_z\rangle\approx\langle I^0_z\rangle=g_n\beta_n I(I+1)B_0/3kT$, so that B_n is very small ($B_n\approx 7$ nT for ^{7}Li at room temperature) and can be neglected in Eq. (1). This situation corresponds to the standard unshifted ESR lines of lithium particles studied in Sec. III. The nuclear field can be enhanced by DNP (Overhauser effect),[6,18] and the resulting shift of the ESR line is now given in this case by the general expression:[23,35]

$$\Delta B_{\mathrm{ov}}=B_n=\Delta B^{\max}_{\mathrm{ov}}\frac{q}{1+q+r(B_0+B_n-h\nu/g\beta)^2}, \tag{10}$$

with $q=\gamma^2T_1T_2B_1^2$ and $r=\gamma^2T_2^2$. The parameter $\Delta B^{\max}_{\mathrm{ov}}$ represents the highest nuclear field achievable under given B_0 and T conditions:

$$\Delta B^{\max}_{\mathrm{ov}}=\frac{I(I+1)NAfB_0}{3kT}. \tag{11}$$

where f is the leakage factor reflecting the efficiency of the electron-nuclear relaxation mechanism T_x ($\Delta m_s=\pm1$, $\Delta m_I=\mp1$) responsible for the nuclear polarization, which compete with other relaxation mechanisms (labeled T_{1n}):[31]

$$f=\frac{1/T_x}{1/T_x+1/T_{1n}}. \tag{12}$$

It is important to note that Eq. (10) is a third degree equation which may have either three or one solutions for B_n, depending on the fact that the critical inequality [Eq. (2)] is satisfied or not.[23] In most cases however $\Delta B^{\max}_{\mathrm{ov}}$ and the relaxation time T_2 are not large enough to satisfy Eq. (2), so that Eq. (10) has only one solution for B_n and the ESR line is only shifted and distorted by the DNP.[23] This situation holds for lithium metal at room temperature. The monostable nuclear field can be quenched by a rf field, which is at the origin of the ENDOR response studied in Sec. IV.

An interesting situation arises when $\Delta B^{\max}_{\mathrm{ov}}$ and T_2 are sufficiently large to satisfy Eq. (2) and to give three solutions for B_n in Eq. (10). In this case the ESR line is not only shifted, it is also strongly distorted and becomes dependent on the field sweep direction because of the bistable character of the nuclear field (two values of B_n are stable and the third one is unstable).[23] We previously proposed to refer to this

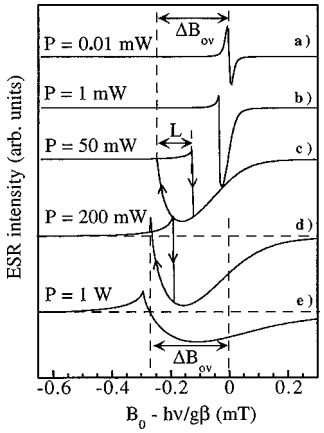

FIG. 8. Example of calculated ESR spectra at different microwave power values for a homogeneous population of submicronic lithium particles. $T=4$ K; $T_1=T_2=0.5\times10^{-6}$ s; $I(I+1)NAf=200$ MHz. ΔB_{ov} and L represent the nuclear field and the hysteresis width, respectively.

situation as bistable conduction electron spin resonance (BCESR).[36] Metallic lithium clearly exhibits this bistable behavior at liquid-helium temperature.[26] All these features are accounted for in the following expression for the ESR line shape:[23]

$$I_{ESR}(B_0)=-I_0\frac{(\gamma T_2)^3 B_1(B_0+B_n-h\nu/g\beta)}{[1+q+r(B_0+B_n-h\nu/g\beta)^2]^2}. \quad (13)$$

An illustration of Eq. (13) is shown in Fig. 8 which describes the theoretical behavior of the ESR line at low temperature for a typical submicronic lithium particle with $T_1=T_2=0.5\times10^{-6}$ s and $I(I+1)NAf=200$ MHz [see Eq. (11)]. The ESR line is unshifted and undistorted only at very low microwave power P [Fig. 8(a)]. Increasing P results first in a shift ΔB_{ov} of the resonance and a distortion of the line shape, with no hysteresis as B_n still remains monostable [Fig. 8(b)]. At higher microwave power, the line distortion still increases while a hysteresis of width L appears [Fig. 8(c)], which reaches a maximum at an optimum value of P, then decreases upon further increasing P [Fig. 8(d)] and vanishes at high microwave power, leaving a very distorted ESR line without hysteresis [Fig. 8(e)]. In a bistable regime, the Overhauser shift ΔB_{ov} is given by the spacing between the center of the unshifted resonance line and the field at which the decreasing sweep ESR trace reaches the baseline (Fig. 8). This shift is related to the microwave power P by[6,18]

$$\Delta B_{ov}=\Delta B_{ov}^{max}\frac{P}{u+P}, \quad (14)$$

with $u=K/\gamma^2T_1T_2$.

It is worth noting that the ESR line shape and the hysteresis strongly depend on ΔB_{ov}^{max} and T_2, so that a small decrease of one of these two parameters may quench the bistability and the hysteresis.[24] Figures 9(a) and 10(a) show the calculated effect of variations of T_2 and ΔB_{ov}^{max} on the microwave power dependence of the Overhauser shift ΔB_{ov}. The curve $\Delta B_{ov}=f(P)$ is sensitive to T_2 essentially at low P values while a modification of ΔB_{ov}^{max} affects the shift at high P values. Thus the quantities T_2T_1 and ΔB_{ov}^{max} can be determined from experimental plots of Eq. (14). Assuming $T_1=T_2$, the ESR spectrum can be calculated with Eq. (13). The sensitivity of the ESR line shape to variations of T_2 and ΔB_{ov}^{max} at low microwave power are shown in Figs. 9(b) and 10(b), respectively. It is remarkable that the ESR line characterized by $T_2\approx0.5\times10^{-6}$ s is monostable and only distorted at 1 mW [Figs. 8 and 9(b)] while it exhibits a significant hysteresis when T_2 is increased by a factor 2 [Fig. 9(b)]. The same effect is observed with an increase of ΔB_{ov}^{max}. It is however less pronounced as a relatively important increase of this parameter is necessary to affect significantly the line shape [Fig. 10(b)]. As shown in the next part, the two popu-

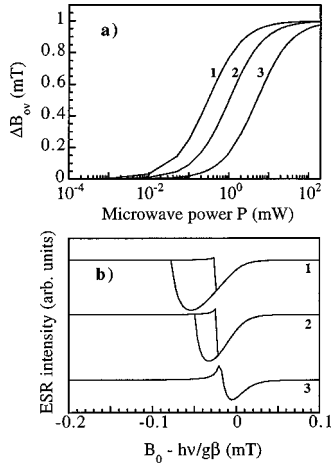

FIG. 9. Influence of the relaxation time T_2 on the BCESR line shape for a homogeneous population of submicronic lithium particles. $T=4$ K; $\Delta B_{ov}^{max}=0.1$ mT, corresponding to $I(I+1)NAf=75$ MHz; (a) microwave power dependence of the Overhauser shift ΔB_{ov}. (b) Simulations of the BCESR spectra at $P=1$ mW. Case 1: $T_2=2.1\times10^{-6}$ s, $u=0.3$ mW; case 2: $T_2=1.1\times10^{-6}$ s, $u=1$ mW; case 3: $T_2=0.5\times10^{-6}$ s, $u=5$ mW.

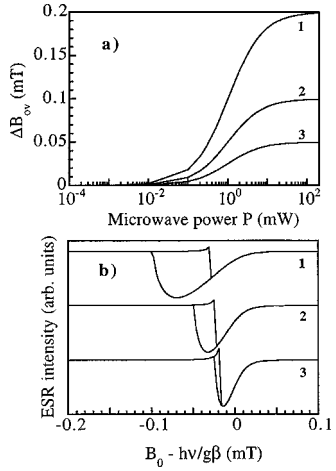

FIG. 10. Influence of ΔB_{ov}^{max} [or $I(I+1)NAf$] on the BCESR line shape for a homogeneous population of submicronic lithium particles. $T=4$ K, $u=1$ mW, $T_2=1.1\times10^{-6}$ s. (a) Microwave power dependence of the Overhauser shift ΔB_{ov}. (b) Simulations of the BCESR spectra at $P=1$ mW. Case. 1: $\Delta B_{ov}^{max}=0.2$ mT, corresponding to $I(I+1)NAf=150$ MHz. Case 2: $\Delta B_{ov}^{max}=0.1$ mT, corresponding to $I(I+1)NAf=75$ MHz. Case 3: $\Delta B_{ov}^{max}=0.05$ mT, corresponding to $I(I+1)NAf=37.5$ MHz.

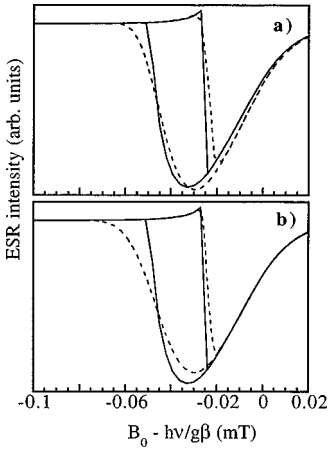

FIG. 11. Effect of a distribution of parameters T_2 and $I(I+1)NAf$ on the BCESR line shape. Full lines: spectra calculated with $T=4$ K, $P=1$ mW, $T_2=1.1\times10^{-6}$ s, $I(I+1)NAf=75$ MHz. Dotted lines: spectra calculated with distributions of parameters: (a) distribution of T_2, with $\sigma_{T_2}=0.3\times10^{-6}$ s; (b) distribution of $I(I+1)NAf$, with $\sigma_{I(I+1)NAf}=20$ MHz.

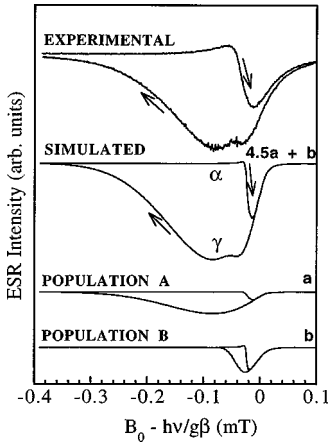

FIG. 12. Experimental and calculated BCESR spectrum of a LiH powder sample irradiated during 0.25 h. $T=4$ K, $P=0.5$ mW. The simulated BCESR spectrum is the sum of the contributions of populations A and B, calculated with parameters given in Table I.

lations A and B of lithium particles exhibit very different BCESR line shapes, which permit accurate measurements of T_2 and $I(I+1)NAf$.

Another aspect of BCESR is the fact that the line shape does not only depend on the values of these parameters, but also on their distributions. The ESR spectrum is a sum over all the particles of a population, which may exhibit distributions of size and shape.[37] Thus the overall CESR intensity $I^{\mathrm{pop}}(B_0)$ of a population is obtained by summing the individual contributions $I_{\mathrm{ESR}}(B_0,X)$ of each particle given by Eqs. (13) and (10), with $X=T_2$ or $I(I+1)NAf$, weighed by the probability $p(X)dX$ or occurrence of each value of X:

$$I^{\mathrm{pop}}(B_0)=\int_{X_{\min}}^{X_{\max}} p(X)I_{\mathrm{ESR}}(B_0,X)dX. \tag{15}$$

Since the actual distribution $p(X)$ is not known, the most usual Gaussian function was chosen:

$$p(X)=\frac{1}{\sigma\sqrt{2\pi}}\exp\left[-\left(\frac{X-\langle X\rangle}{\sigma\sqrt{2}}\right)^2\right], \tag{16}$$

where $\langle X\rangle$ is the mean value of X and σ its standard deviation. For computational reasons, the integration limits $X_{\min}$ and $X_{\max}$ were chosen so that $\forall X\in[X_{\min},X_{\max}]$, $p(X)\geqslant10^{-3}/\sigma\sqrt{2\pi}$, and the integration of Eq. (15) was achieved by the usual Simpson algorithm. Two examples of calculated effects of distribution of T_2 and $I(I+1)NAf$ parameters are shown in Fig. 11. Full lines represent the BCESR spectra calculated at 4 K and $P=1$ mW for a homogeneous population of lithium particles characterized by $T_2=10^{-6}$ s and $I(I+1)NAf=75$ MHz. The dotted lines represent the same spectra calculated with Gaussian distributions of these parameters, with standard deviations $\sigma_{T_2}=0.3\times10^{-6}$ s [Fig. 11(a)] and $\sigma_{I(I+1)NAf}=20$ Mhz [Fig. 11(b)].

B. BCESR of populations A and B

The consequence of the preceding considerations is that the two populations, characterized by specific T_2 values, should be distinguishable by their BCESR spectra. This is shown in Fig. 12, which represents a BCESR spectrum at 4 K and $P=0.5$ mW for a LiH powder sample irradiated during 0.25 h. The unsaturated ESR spectrum ($P\leqslant0.5\,\mu$W, not shown) was composed of 15 and 85% of populations A and B, respectively. The apparent spin-spin relaxation times $T_2^*=2/\sqrt{3}\,\gamma\Delta B$ deduced from the peak-to-peak linewidths are given in Table I. Bistability and hysteresis appear at higher microwave power (Fig. 12). However, the experimental spectrum is significantly different from the theoretical one described in Fig. 8: (i) a shoulder in the decreasing field spectrum reflects the different BCESR line shapes of the two populations; (ii) there is no abrupt transition in the increasing field spectrum, and the decreasing field spectrum extends to much lower fields than theoretical spectra, these two features reflecting the distributions of the ESR parameters (see Fig. 11); (iii) the most striking feature is that a broad hysteresis is always present at a microwave power of 0.5 mW at which a hysteresis is not predicted if we consider the apparent relaxation times $T_2^*(A)=0.41\times10^{-6}$ s and $T_2^*(B)=0.1\times10^{-6}$ s deduced from the unsaturated ESR linewidth (see Fig. 8).

Figure 12 also shows the spectrum simulated as the sum of two BCESR lines, one for each type of population. The simulation was very sensitive to the quantities T_2 and $I(I+1)NAf$, which play a different role in the shape of the spectrum. The simulation parameters are listed in Table I. The most interesting result is that the relaxation times deduced from the simulation, $T_2(A)=4.8\times10^{-6}$ s and $T_2(B)=0.9\times10^{-6}$ s are much larger than the T_2^* values deduced from the ESR linewidths. This feature can only be explained if the unsaturated ESR line exhibits a residual broadening by magnetic field inhomogeneities or modulation effects, giving a smaller apparent T_2^*. It is remarkable that the T_2 value of population A is very close to that measured in LiF:Li by Cherkasov *et al.* by spin-echo methods ($T_2\approx5\times10^{-6}$ s below 100 K),[38] indicating that we are probably dealing with the same type of Li particles in LiH:Li and LiF:Li. The second feature revealed by the simulation is that the DNP is very similar for the two populations, with $I(I+1)NAf=110$ and 140 MHz for populations A and B, respectively.

TABLE I. Examples of ESR and BCESR parameters at low temperature of lithium particles in a LiH powder sample irradiated 0.25 h. The parameters deduced from the BCESR spectra are compared with those of Li_2O:Li.

Compound	Method	Parameter	Population A	Population B
	ESR	weight (%)	15	85
	($P=5\ \mu$W, $T=4$ K)	ΔB (μT)	15.9	66.6
		T_2^* (10^{-6} s)	0.41	0.10
LiH:Li	$\Delta B_{ov}=f(P)$	T_2 (10^{-6} s)	4.8 ± 0.3	0.9
	($T=20$ K)	$I(I+1)NAf$ (MHz)	<330	<215
	BCESR	T_2 (10^{-6} s)	4.8	0.9
	($P=0.5$ mW, $T=4$ K)	$\langle I(I+1)NAf\rangle$ (MHz)	110	140
		$\sigma_{I(I+1)NAf}$ (MHz)	78	35
	BCESR	T_2 (10^{-6} s)	0.49	0.2
Li_2O:Li[a]	($P=25$ mW, $T=4$ K)	$\langle I(I+1)NAf\rangle$ (MHz)	240	240
		$\sigma_{I(I+1)NAf}$ (MHz)	35	35

[a]Reference 26.

Accurate simulations were only obtained with distributions of DNP parameters $I(I+1)NAf$ (Table I and Fig. 12), as a distribution of T_2 could not reproduce the experimental line shape. It is interesting to note that population A exhibits a much broader distribution of DNP than population B. Since $I(I+1)NA$ is equal to 650 MHz in metallic lithium, the observed distribution of DNP is only due to the leakage factor f [see Eq. (12)], which amounts to $f=0.17$ (with $\sigma_f=0.12$) for population A, and $f=0.22$ (with $\sigma_f=0.05$) for population B. A leakage factor $f=1$ corresponds to a nuclear relaxation via conduction electrons. Thus the observed leakage factors and their distributions reflect the competition, in each particle, between the different relaxation mechanisms,[31] and their variation from one particle to the other.

Another proof of the existence of two populations of lithium particles is the variation of the Overhauser shift ΔB_{ov} versus the incident microwave power, shown in Fig. 13. These measurements were made at 20 K instead of 4 K in order to decrease the relaxation time T_x sufficiently to permit multiple forward and backward sweeps of B_0 in a reasonable time. The experimental variation is significantly different from the theoretical ones described in Figs. 9(a) and 10(a), and reflects the different behaviors of populations A and B. At low microwave power ($P<0.5$ mW) the ESR spectrum is dominated by the narrow line of population A characterized by a long T_2 [see Fig. 9(a) for the effect of T_2]. At $P>0.5$ mW, ΔB_{ov} steeply decreases and next slowly increases (Fig. 13), which is due to the strong broadening of the BCESR line A and a corresponding decrease of its amplitude. The consequence is that the BCESR line B is narrower than line A at high microwave power, and thus dominates the spectrum. Simulations of the low and high P portions of the experimental curve give $T_2=(4.8\pm0.3)\times10^{-6}$ s and $T_2=0.9\times10^{-6}$ s for populations A and B, respectively (dotted and discontinuous lines in Fig. 13). These values are exactly the same as those obtained by simulation of the BCESR spectrum (Fig. 12 and Table I).

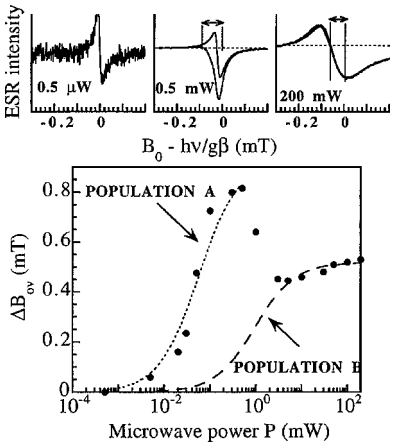

FIG. 13. Microwave power dependence of the Overhauser shift ΔB_{ov} in a powder LiH sample irradiated during 0.25 h. $T=20$ K. Dotted line (population A): calculated with $T_2=(4.8\pm0.3)\times10^{-6}$ s and $I(I+1)NAf<330$ MHz, discontinuous line (population B): calculated with $T_2\approx0.9\times10^{-6}$ s and $I(I+1)NAf<215$ MHz. Three examples of ESR spectra at different microwave power are shown at the top of the figure.

We have noted in Sec. III that the ESR line broadens upon annealing treatments, and that population A decreases more rapidly than population B (Fig. 3). However, examination of the saturated ESR line at low temperature, in normal conditions of bistability, reveals a deeper effect of the annealing treatment than a simple line broadening. Figure 14 shows the ESR spectrum at 4 K and $P=0.5$ mW of an irradiated sample annealed during 500 min at 180 °C. It appears that the line is only slightly distorted by the DNP and the hysteresis is extremely reduced. We could not obtain an accurate

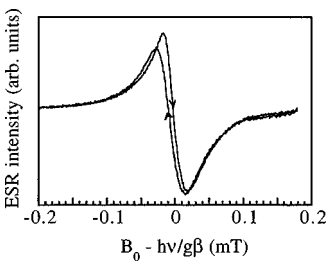

FIG. 14. BCESR spectrum at $P=0.5$ mW of the sample of Fig. 1(b), irradiated during 3 h and treated 500 min at 180 °C.

simulation for this spectrum, most probably because of a very broad, non-Gaussian distribution of parameters. However, the mean values of the parameters was found to be $T_2 \approx 0.2 \times 10^{-6}$ s and $I(I+1)NAf \approx 120$ MHz. The decrease of T_2 might be due to the increase of the spin relaxation by the particle surface due to the reduced particle size. This effect generally occurs for particles smaller than about 300 nm.[37,39,40]

VI. DISCUSSION

The results of Secs. IV and V show that ENDOR and BCESR are much more selective than conventional ESR spectroscopy, since well defined populations of metallic lithium particles were detected from ESR spectra having only a single symmetrical line. The selectivity of BCESR is particularly interesting since it permits accurate measurements of magnetic parameters of metallic particles, which reflect the history of the particles and the nature of the host matrix. This can be checked by comparing Li particles in LiH:Li (UV irradiation) and Li_2O:Li (electron irradiation).[26] In both cases only a single symmetrical ESR line with the same linewidth is observed, while the BCESR spectrum reveals the presence of two distinct populations of particles. However, the magnetic parameters measured for the two populations (Table I) are clearly different in Li_2O:Li (Ref. 26) and LiH:Li: (i) the DNP in Li_2O:Li is about twice that of LiH:Li; (ii) the two populations of each matrix exhibit about the same DNP, and are characterized by different T_2 values; (iii) T_2 values are smaller in Li_2O:Li than in LiH:Li. These results indicate that the production of a dual population of lithium particles by irradiation seems to be a general feature (see also Refs. 7, 11, and 16), however, their magnetic parameters are matrix dependent and reflect the history of the samples. The actual values of $I(I+1)NAf$ being determined by the leakage factor f [see Eq. (12)], the values $f=0.37$ and $f \approx 0.2$ found for Li_2O:Li (Ref. 26) and LiH:Li, respectively, indicate that the nuclear relaxation times competing with the relaxation via conduction electrons are matrix dependent, and that they are almost identical for the two populations of particles in each type of matrix.

We address now the problem of the crystallographic structure of lithium metal in each population. Metallic lithium at ambient pressure has the body-centered-cubic (bcc) structure at $T > 72$ K. A martensitic transformation below 80 K gives low temperature $9R$ phase of lithium characterized by a nine-layer sequence of close-packed planes (ABCBCACAB).[41] Additionally the $9R$ phase becomes partially face-centered-cubic (fcc) upon heating above 80 K, before reverting to the high-temperature bcc phase.[42] At room temperature the fcc phase is stable at pressures larger than 6.3 GPa.[32] Each Li atom has 8 first neighbors in the bcc phase and 12 first neighbors in the close-packed $9R$ and fcc phases. The site symmetry is cubic in the bcc and fcc phases, and axial in the $9R$ phase. Consequently, Li nuclei may experience an electric-field gradient only in the hcp phase. Thus it appears likely that population B belongs to the $9R$ phase owing to the presence of a quadrupole structure in its nuclear-magnetic-resonance spectrum. Very recent ^{7}Li NMR measurements in Li_2O:Li single crystals showed the presence of two NMR signals with different Knight shifts, revealing the presence of two distinct metallic phases,[13] characterized by very distinct ESR spectra.[11] One of these ESR lines exhibited the same temperature variations of the linewidth and the intensity as those found for population B in LiH:Li. It is thus tempting to conclude that the large Li particles in Li_2O:Li (Ref. 13) and the Li particles of population B in LiH:Li belong to the $9R$ phase. This hypothesis should be tested by ENDOR. However, the signal-to-noise ratio of the ENDOR response of Li_2O:Li was too low to reveal any structure.[26]

We must consider two possible cubic structures (bcc or fcc) for Li particles of population A owing to the lack of quadrupole interaction of their nuclear magnetic resonance. Despite the fact that only the bcc phase is stable at ambient temperature and pressure, it is tempting to assign population A to the fcc phase. A first reason is that fcc particles have already been observed by x-ray diffraction in LiF:Li,[3] and the T_2 values measured in this compound[38] were nearly identical with those found in this work for population A. Another reason is purely geometrical. It is well known that ionizing radiations produce F centers (electron trapped at anion vacancies) with displacement of interstitial atoms.[43] In LiH the interstitial H atoms give hydrogen gas in the form of bubbles in the crystals.[44] Thus sufficiently large aggregates of F centers may be seen as a lattice of $n\mathrm{Li}^+$ ions with n electrons, giving metallic Li precipitates. The Li^+ ions of the rock-salt structure of LiH and LiF occupy a fcc lattice which thus plays the role of a template for the formation of fcc Li particles by electron capture from F centers. This phase should normally transform into bcc Li metal owing to the unstability of fcc Li metal at ambient pressure. This is also true for the $9R$ phase, stable below 80 K. However, it is important to note that electron capture by a Li^+ lattice of volume V_0 gives metallic Li particles of volume $V > V_0$. For fcc, $9R$, and bcc Li metal, the relative volume expansion $\Delta V/V_0$ in LiH (with $\Delta V = V - V_0$) is equal to 0.254, 0.275, and 0.291, respectively, so that fcc Li are the particles which experience the smallest pressure by the surrounding lattice. Consequently fcc Li particles should be more stable than bcc Li in LiH.

VII. CONCLUSION AND PROSPECT

Metallic lithium colloïds created by UV irradiation of lithium hydride were investigated in this work as a model system by combining classical ESR, ENDOR, and BCESR spectroscopies. Compared with standard ESR of conduction electrons, which is only sensitive to the size of the particles with respect to the skin depth of the metal, ENDOR and BCESR are techniques of high selectivity and resolution which allowed us to distinguish two crystallographically different phases of lithium from a single structureless ESR line. The following conclusions can be drawn from the present work:

(i) It is now established that the deviation from the Lorentzian shape of the wings of the ESR line of lithium metal, often mentioned in the literature, is the manifestation of the coexistence of two crystallographically different phases of the metal, as previously proposed in lithium fluoride.[8]

(ii) ENDOR spectroscopy shows that one population of particles probably belongs to the $9R$ close-packed phase, the

other population being cubic, most probably of the face-centered-cubic type.

(iii) At low temperature, the ESR line of conduction electrons exhibits a pronounced bistable hysteresis which shows that the electronic relaxation time T_2 of lithium is much larger than that deduced from the ESR linewidth, demonstrating also the inhomogeneous character of the latter. The cubic and noncubic phases of lithium in LiH are characterized by $T_2 \approx 5 \times 10^{-6}$ s and $T_2 \approx 10^{-6}$ s, respectively. These small differences of T_2 are sufficient to give two distinguishable BCESR spectra.

(iv) The two populations of particles exhibit a broad distribution of their nuclear relaxation times.

Finally, it is worth mentioning that the combination of highly selective ENDOR and BCESR spectroscopies might be useful for studying the behavior of systems involving metallic lithium, such as secondary lithium batteries. It is well established that the life cycle of these batteries is limited by the lack of reversibility of the Li anode related to the morphology of the electrodeposited lithium metal.[17] The formation of dendrites of about 4–5 μm width usually occurs at the anode-electrolyte interface. Standard ESR spectroscopy can hardly distinguish between electrodeposited lithium dendrites and the bulk lithium of the anode. We believe that BCESR and ENDOR are sufficiently sensitive, resolutive, and selective to distinguish the different types of metallic lithium deposited during the multiple cycles of the battery.

ACKNOWLEDGMENTS

We are grateful to D. Simons for technical assistance. Laboratoire de Chimie Appliquée de l'Etat Solide is a ''Unité Associée au Center National de la Recherche Scientifique UMR-7574-CNRS.''

*Author to whom correspondence should be addressed. Electronic address: gourierd@ext.jussieu.fr

[1] G. Feher and A. F. Kip, Phys. Rev. **98**, 337 (1955); F. J. Dyson, *ibid.* **98**, 349 (1955).
[2] A. E. Hughes and S. C. Jain, Adv. Phys. **28**, 717 (1979), and references therein.
[3] M. Lambert and A. Guinier, C. R. Hebd. Seances Acad. Sci. **246**, 1678 (1958).
[4] P. J. Ring, J. G. O'Keefe, and P. J. Bray, Phys. Rev. Lett. **1**, 453 (1958).
[5] Y. W. Kim, R. Kaplan, and P. J. Bray, Phys. Rev. **117**, 740 (1960).
[6] Ch. Ryter, Phys. Rev. Lett. **5**, 10 (1960).
[7] M. Lambert, Ch. Mazières, and A. Guinier, J. Phys. Chem. Solids **18**, 129 (1961).
[8] A. Stesmans and Y. Wu, J. Phys. D **21**, 1205 (1988).
[9] K. Noda, K. Ushida, T. Tanifuji, and S. Nasu, Phys. Rev. B **24**, 3736 (1981); K. Noda, Y. Ishii, H. Matsui, and H. Watanabe, Radiat. Eff. **97**, 297 (1986).
[10] P. Vajda and F. Beuneu, Phys. Rev. B **53**, 5335 (1996).
[11] F. Beuneu and P. Vajda, Phys. Rev. Lett. **76**, 4544 (1996).
[12] F. Beuneu, P. Vajda, G. Jaskierowicz, and M. Lafleurielle, Phys. Rev. B **55**, 11 263 (1997).
[13] F. Beuneu, P. Vajda, and O. J. Zogal, Nucl. Instrum. Methods Phys. Res. B **141**, 241 (1998).
[14] R. Kubo, J. Phys. Soc. Jpn. **17**, 975 (1962); A. Kawabata, *ibid.* **24**, 902 (1970).
[15] J. P. Borel, C. Borel-Narbel, and R. Monot, Helv. Phys. Acta **47**, 537 (1974); S. Pasche and J. P. Borel, Solid State Commun. **58**, 865 (1986); A. Chatelain, J. L. Millet, and R. Monot, J. Appl. Phys. **47**, 3670 (1976).
[16] C. Taupin, J. Phys. Chem. Solids **28**, 41 (1967).
[17] R. Selim and P. Bro, J. Electrochem. Soc. **121**, 1457 (1974); I. Yoshimatsu, T. Hirai, and J. Yamaki, *ibid.* **135**, 2422 (1988); A. Tudela Ribes, P. Beaunier, P. Willmann, and D. Lemordant, J. Power Sources **58**, 189 (1996).
[18] A. Overhauser, Phys. Rev. **92**, 411 (1953).
[19] M. Gueron and Ch. Ryter, Phys. Rev. Lett. **3**, 338 (1959).
[20] G. Feher and R. A. Isaacson, J. Magn. Reson. **7**, 111 (1972).
[21] G. Denninger, Bruker Rep. **1/1987**, 18 (1987).
[22] G. Denninger and D. Reiser, Phys. Rev. B **55**, 5073 (1997), and references therein.
[23] E. Aubay and D. Gourier, Phys. Rev. B **47**, 15 023 (1993).
[24] L. Binet and D. Gourier, J. Phys. Chem. **100**, 17 630 (1996).
[25] L. Binet, D. Gourier, and C. Minot, J. Solid State Chem. **113**, 420 (1994).
[26] C. Vigreux, L. Binet, and D. Gourier, J. Phys. Chem. B **102**, 1176 (1998).
[27] W. T. Doyle, D. J. E. Ingram, and M. J. A. Smith, Phys. Rev. Lett. **15**, 497 (1959).
[28] P. Damay, and M. J. Sienko, Phys. Rev. B **13**, 603 (1976).
[29] R. H. Webb, Phys. Rev. **152**, 225 (1967).
[30] G. O. Berim, F. G. Cherkasov, E. G. Kharakhashyan, and Y. I. Talanov, Phys. Status Solidi A **40**, K53 (1977).
[31] A. Abragam, *Principle of Nuclear Magnetism* (Clarendon, Oxford, 1961).
[32] R. Bertani, M. Mali, J. Roos, and D. Brinkmann, J. Phys.: Condens. Matter **2**, 7911 (1990).
[33] We have verified that the second-order contribution of the quadrupole interaction has a negligible effect on the spectrum. It is of the order of $\nu_q^2/10\nu_{\mathrm{Li}} \approx 10$ kHz, a value much smaller than the ENDOR linewidth $\Delta\nu \approx 170$ kHz.
[34] J. Winter, *Magnetic Resonance in Metals* (Clarendon, Oxford, 1971).
[35] J. I. Kaplan, Phys. Rev. **99**, 1322 (1955).
[36] D. Gourier, E. Aubay, and J. Guglielmi, Phys. Rev. B **50**, 2941 (1994).
[37] K. Saiki, T. Fujita, Y. Shimizu, S. Sakoh, and N. Wada, J. Phys. Soc. Jpn. **32**, 447 (1972).
[38] F. G. Cherkasov, E. G. Kharakhash'Yan, L. I. Medvedev, N. I. Novosjelov, and Y. I. Talanov, Phys. Lett. **63A**, 339 (1977).
[39] M. Y. Gen and V. I. Petinov, Zh. Eksp. Teor. Fiz. **48**, 29 (1965) [Sov. Phys. JETP **21**, 19 (1965)].
[40] S. Sako, J. Phys. Soc. Jpn. **59**, 1366 (1990).
[41] A. W. Overhauser, Phys. Rev. Lett. **53**, 64 (1984); W. Schwarz and O. Blaschko, *ibid.* **65**, 3144 (1990).
[42] H. G. Smith, R. Berlinger, J. D. Jorgensen, M. Nielsen, and J. Trivisomo, Phys. Rev. B **41**, 1231 (1990).
[43] E. Sonder and W. A. Sibley, in *Point Defects in Solids*, edited by J. H. Crawford and L. M. Slifkin (Plenum, New York, 1972).
[44] P. C. Souers, T. S. Blake, R. M. Penpraze, and C. Cline, J. Phys. Chem. Solids **30**, 2649 (1969); T. Miki and M. Ikeya, J. Phys.: Condens. Matter **13**, 4439 (1980).